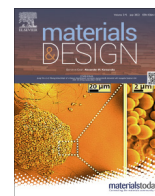Contents lists available at ScienceDirect

Materials & Design

journal homepage: www.elsevier.com/locate/matdes

Effect of composition and nanostructure on the mechanical properties and thermal stability of $Zr_{100-x}Cu_x$ thin film metallic glasses

Andrea Brognara [a,*], James P. Best [a], Philippe Djemia [b], Damien Faurie [b], Gerhard Dehm [a,*], Matteo Ghidelli [a,b,*]

[a] Max-Planck-Institut für Eisenforschung GmbH, Düsseldorf, 40237, Germany
[b] Laboratoire des Sciences des Procédés et des Matériaux (LSPM), CNRS, Université Sorbonne Paris Nord, Villetaneuse, 93430, France

HIGHLIGHTS

- The mechanical properties and thermal stability of nanostructured columnar $Zr_{100-x}Cu_x$ thin film metallic glasses were investigated and compared to those of homogeneous films.
- Crystallization temperature, hardness and elastic modulus were found to be mostly dependent on composition and local atomic order rather than from film nanostructure.
- Viscoplastic behavior show high influence on both film composition and nanostructure, with columnar Zr-rich films showing higher tendency toward serrated flow deformation.
- Resistance to cracking is higher for Cu-rich and homogeneous films thanks to the higher density of full icosahedral atomic packing, while interfaces favored crack initiation.

GRAPHICAL ABSTRACT
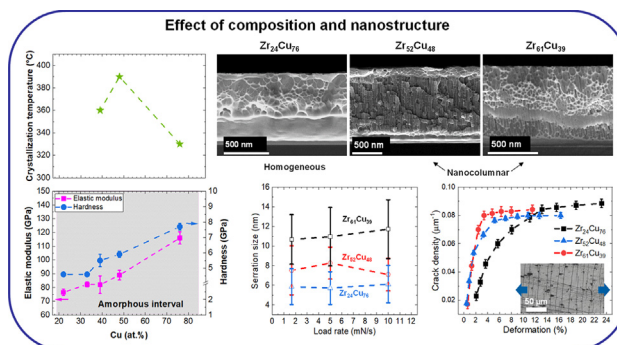
ABSTRACT

Thin film metallic glasses (TFMGs) are a novel class of materials showing a mutual combination of large plastic deformation in tension (>10% strain) and superior yield strength up to ∼ 3.5 GPa, which make them ideal candidates for applications such as flexible electronics. Nevertheless, a clear relationship between the atomic structure and mechanical properties of TFMGs has not yet been achieved. In particular, the role of composition in determining a different local atomic order and the effect of nanostructure on TFMGs properties must be further investigated. In this work, the mechanical properties and thermal stability of several amorphous $Zr_{100-x}Cu_x$ TFMGs with either compact or fine columnar nanostructure were studied. The mediating role of composition in controlling crystallization temperature and hardness is here reported, which was found to increase from 4.6 to 7.7 GPa with increasing Cu content from 26 to 76 at.%. Moreover, plastic behavior and fracture resistance are shown to be highly dependent on both composition and nanostructure, with the Cu-rich and homogeneous film able to withstand elongation up to 2% strain before crack initiation. These results underline how atomic structure changes induced

* Corresponding authors.
  E-mail addresses: a.brognara@mpie.de (A. Brognara), dehm@mpie.de (G. Dehm), matteo.ghidelli@lspm.cnrs.fr (M. Ghidelli).

by composition can effectively influence TFMG properties, while demonstrating an approach to tune their behavior for various technological applications.

1. Introduction

Bulk metallic glasses (BMGs) represent an exciting class of metallic alloys with unique mechanical properties such as elevated yield strength up to 2 GPa combined with large elastic deformability $\geq$ 2% [1]. Unfortunately, the application of BMGs as structural materials is hindered by their lack of ductility at room temperature due to the activation of narrow $\sim$ 10 nm thick shear bands (SBs) during plastic deformation in tension [2,3]. However, this macroscopically brittle behavior can be drastically reduced by decreasing the sample size down to the micrometer scale [4]. Indeed, thanks to the activation of these mechanical size effects, catastrophic SBs can be delayed or even suppressed. For these reasons, thin film metallic glasses (TFMGs) report high hardness in combination with impressive yield strength up to $\sim$ 3.5 GPa, but also a retained ductility, sustaining plastic deformation up to $\sim$ 10% strain in tension [5]. These properties make TFMGs outstanding candidates for applications such as flexible or wearable electronics [6]. Molecular dynamics (MD) simulations and experimental works on metallic glasses, including ZrCu alloys, have shown that composition affects local atomic order, which can significantly influence the mechanical behavior [7-9] and thermal stability [10-13]. However, a strong fundamental understanding of the link between atomic structure and mechanical properties has not yet been achieved. For example, a key unanswered question concerns the precise role of metallic glass composition, affecting atomic structure and consequent influence on mechanical properties and thermal stability against crystallization.

Binary ZrCu alloys represent an ideal candidate to address this fundamental question, due to their lower complexity compared to multi-component alloys, their wide amorphization range from $\sim$ 30 to $\sim$ 85 at.% Cu, and the established sensitivity of their properties to composition [7,10]. Moreover, ZrCu TFMGs have been reported to show excellent mechanical properties such as large tensile yielding strength and elongation to failure up to 2.6 GPa and 9% respectively [14].

Recently, attention has also been given to the synthesis of nanostructured MGs, often referred as nanoglasses (NGs), usually obtained by compaction of MG powders [15,16], but also via nanostructured TFMGs reporting columnar morphologies [17,18]. This specific class of amorphous materials show different structural characteristics compared to their homogeneous counterparts, such as an increased free volume content due to the higher degree of disorder present at glass-glass interfaces [15,16]. The nanostructure can also influence the mechanical behavior, in particular the plasticity, where uniform plastic deformation occurs in contrast to homogeneous MGs [16,19-21].

In this work, the effect of composition and nanostructure on mechanical properties and thermal stability of ZrCu TFMGs is studied extensively, combining different characterization techniques. Films having either a homogeneous or a nanocolumnar morphology, with average column diameter of $\sim$ 20–50 nm, were deposited by magnetron sputtering enabling precise control over composition through fine regulation of process parameters. Scanning electron microscopy (SEM) and electron dispersive X-ray spectroscopy (EDX) were used to investigate sample morphology and chemistry, while material structure, thermal stability and devitrification processes were studied by X-ray diffraction (XRD) (i.e. from room temperature up to 600 °C). Hardness (H) and elastic modulus (E) were evaluated by nanoindentation and surface Brillouin spectroscopy (SBS).

A comparison is then made with previously reported mechanical properties and crystallization temperature of homogeneous ZrCu TFMGs [7,10,11] and the effect of nanostructure is discussed. In addition, deep investigations on the films plastic and viscoplastic behavior by nanoindentation and a study of the fracture resistance of ZrCu TFMGs during tensile tests performed on flexible substrates are presented. The obtained results are discussed both on the basis of the effect of composition and related changes in the local atomic order, together with the role played by nanostructure in influencing films mechanical behavior. Overall, this study paves the way for a better design of ZrCu TFMGs and their application in growing domains such as high resistance coatings and stretchable electronics.

2. Experimental

2.1. Film synthesis

ZrCu TFMGs were deposited by magnetron sputtering (Bestec GmbH) using pure Cu (99.999% pure) and Zr (99.2% pure) targets both purchased from Kurt J. Lesker®. Cu was placed on a RF cathode due to its higher sputtering rate, while a DC cathode was used for Zr, enabling precise composition control. Prior to deposition the chamber was pumped down to a base vacuum pressure < 10^{-6} Pa, after which Ar gas was introduced at a rate of 20 cm^3/min to reach a target of 0.5 Pa. ZrCu TFMGs were grown on either Si (100), Si (100) coated with 50 nm thick amorphous SiN_x, or on flexible Kapton® substrates. Substrates were placed at a distance of 239 mm from the cathodes and rotated at 30 rpm to obtain higher thickness homogeneity. The control of power values applied to RF and DC cathodes, ranging from 20 to 300 W, enabled a fine tuning of film composition. Films were deposited with thicknesses of both 400 nm and 1 μm, with deposition times varying between 15 min and 1 h.

2.2. Structural characterization

Scanning electron microscopy (Zeiss-Gemini 500 SEM) was used to measure film thickness and inspect morphology, while the atomic composition was determined by energy dispersive X-ray spectroscopy (EDX), setting the acceleration voltage of 15 kV and using the EDAX Genesis spectra analysis software. EDX measurements were performed on several areas of the samples with 1 μm thick film thickness without observable signal from the Si substrate. The deviation between multiple SEM-EDX measurements for a specific ZrCu film composition was always below 0.4 at.%. All EDX data reported in this paper are given in at.%.

Atomic force microscope (AFM) measurements were carried out with a Digital Instruments Dimension 3100 AFM, to evaluate the surface topology and the roughness. The measurements were carried out in tapping mode with a tetrahedral silicon tip of 7 nm diameter. Scans were performed in air at 0.5 Hz.

Structural investigation of the films deposited on Si (100) was carried out by grazing incidence X-ray diffraction (GIXRD, Cu Kα radiation, λ = 0.154 nm), with a Rigaku SmartLab 9 kW diffractometer. Measurements were performed at 45 kV and 200 mA with

XRD acquisition in the 20°-100° 2θ range using continuous scan mode, with step size of 0.01° and scanning speed of 0.75°/min.

Thermal stability and the onset of crystallization were evaluated through acquisition of *in situ* XRD spectra and increasing the temperature from T_{room} up to 600 °C. In order to prevent possible thermally activated interdiffusion phenomena and Zr-Si reactions, these films were deposited on Si (1 0 0) wafers coated with an amorphous SiN$_x$ diffusion barrier layer. The heating ramp was set to 30 °C/min and diffractograms were recorded at constant temperatures every 30 °C. Samples were placed in a stable controlled He atmosphere at 1.35×10^5 Pa to avoid oxidation. Measurements were performed with the same set-up as for the as-deposited films, but using Bragg-Brentano geometry (θ/2θ scan axis) with a shortened range from 25°-90° scanned in continuous mode, a step size of 0.01° and scanning speed of 3°/min. An offset of 3° was introduced to avoid the Si substrate signal.

2.3. Nanoindentation

Nanoindentation tests were carried out using a diamond Berkovich tip (Synton-MDP AG, Switzerland) mounted on a KLA G200 Nanoindenter XP head. Prior to testing, the tip area function was calibrated on fused silica. Measurements performed at room temperature under load-control mode, using continuous stiffness measurement (CSM) method provided values of hardness (*H*) and elastic modulus (*E*) with increasing penetration depth. The allowable maximum drift rate was set to 0.05 nm s^{-1} and the load rate ($\dot{P}/P$) fixed to 0.05 s^{-1}. The maximum indentation depth was limited to 500 nm and values of *H* and *E* were extracted for depths between ∼ 50 nm and 100 nm (i.e. below ∼ 10% of film thickness) to avoid substrate influence, using the Oliver and Pharr method [22].

The time-dependent mechanical response of ZrCu films was analyzed using a standard indentation method imposing different load rates ($\dot{P}/P$). Applied load rate is given by the ratio between maximum load and indentation duration. Maximum target load was fixed to 50 mN (i.e. corresponding to maximum penetration depths of ∼ 550 nm and ∼ 620 nm, depending on film composition) and the total indentation duration varied from 2 to 30 s, resulting in load rate values spanning from 1.6 to 25 mN/s.

2.4. Surface Brillouin spectroscopy (SBS)

SBS experiments were performed in the standard back scattering geometry for opaque materials [23,24], with incident laser beam (single mode solid laser Torus, Quantel) wavelength of λ = 532 nm. The wave vector modulus of the thermally excited surface acoustic waves (SAW) is defined by $Q = 4\pi/\lambda_L \sin(\theta)$. The sound velocity (*V*) of SAW is calculated by the relation $V = 2\pi F/Q$, with *F* being the measured Brillouin frequency shift. In the specific case of TFMGs, elastic properties are defined by only two independent elastic constants C_{11} and $C_{44}=(C_{11}-C_{11})/2$, from which the elastic moduli and Poisson ratio can be calculated. By considering the scattering of light by the ripple mechanism [25] with known mass density (ρ) and thickness (*h*) of the film, the Brillouin spectra can be fit by the power spectrum of the vertical displacement U_z^2 (*z* = 0, F) of the free surface of the film. The mass density of ZrCu TFMGs was evaluated by measuring film mass with a microbalance, while volume was estimated by measuring film thickness by SEM and knowledge of the substrate surface area. This was found to be in good agreement with the rule of mixture based on the film composition (at.%) and Zr, Cu atomic masses. For films with moderate thickness of ∼ 400 nm, several peaks with decreasing intensity are observed in the SBS spectra. The peak of lowest frequency (F_R) is attributed to the Rayleigh surface wave, which

has the particularity to be closely related to the shear sound velocity $V_S=(C_{44}/\rho)^{1/2}$ and shear elastic constant [26], and above to the Sezawa surface waves (S_i) [27].

2.5. Tensile test on flexible substrates

Tensile tests were performed on films deposited on flexible Kapton® substrates, using a 300 N Deben tensile machine combined with a Keyence confocal microscope. The tensile speed was 0.2 mm/min and sample length 30 mm, corresponding to a strain rate of ca. 1.1×10^{-4} s^{-1}. Objectives of 10 × or 20 × magnification were used to visualize a sufficient number of cracks and buckles, in order to determine linear or surface density. Since confocal microscopy acquisitions require a few seconds collection time, tests were stopped for each measurement. The linear density of cracks (aligned orthogonal to the loading direction) and the surface density of buckles were estimated by measuring the number of cracks and buckles over the area of the sample (i.e. 700 μm × 525 μm of size) captured by the microscope objective. These estimates were performed for each applied strain to measure the evolution of these parameters with uniaxial loading.

3. Results and discussion

In this section, the film synthesis strategy is firstly introduced, together with investigation of amorphous structure and morphology by XRD and SEM. The results on thermal stability against crystallization and mechanical properties dependence on composition of ZrCu TFMGs then follows.

3.1. Synthesis of ZrCu TFMGs: Structure and morphology

Fig. 1 shows the XRD spectra of the various as-deposited ZrCu TFMGs. The presence of the broad peaks between 30° and 45° typical of metallic glasses, shows that films are X-ray amorphous within a wide compositional range spanning between 26 and 85 at.% Cu. For Cu contents below 26 at.%, or above 85 at.%, films have a fully crystalline structure in good agreement with reports in literature [11]. An exception is found for the film with 93 at.% Cu, where the amorphous peak at low 2θ is still visible together with
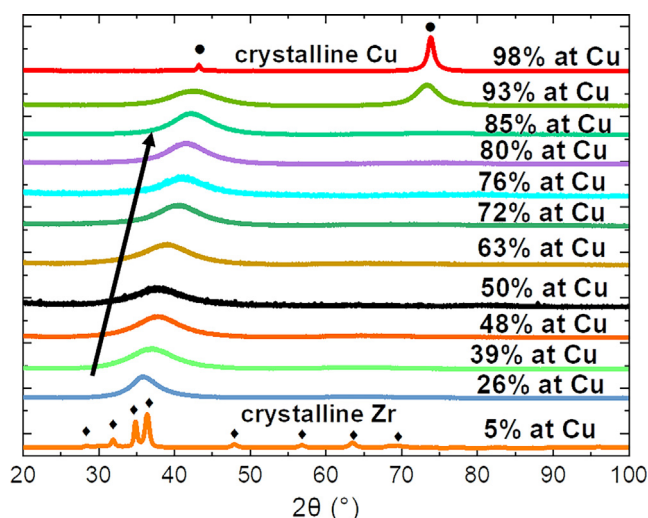

Fig. 1. Influence of composition on ZrCu atomic structure: XRD spectra of ZrCu films with different Cu contents, showing amorphous atomic structure for compositions between 26 and 85 at.% Cu. The shift in peak position toward higher 2θ is due to a decrease of the average atomic distance with Cu enrichment.

a sharper peak at 73° corresponding to Cu $(2\,2\,0)$ phase, suggesting the presence of partial crystallization in an amorphous matrix.

A first direct effect of composition on the atomic structure of amorphous films can be detected by the shift on the peak maxima position towards higher 2θ with increasing Cu content (Fig. 1). This corresponds to a decrease of the average atomic distance [7], which can be calculated through the Ehrenfest equation [28]: $2d\sin(\theta) = 1.23\lambda$, showing that the average atomic distance linearly decreases from ca. 3.08 to 2.63 Å, for Cu contents of 26 at.% and 85 at.% respectively (Fig. S1 in the supplementary), following a similar trend to what was reported by Apreutesei *et al.* [11] and Zeman *et al.* [10]. Films with higher Cu content therefore, have a denser atomic packing. Fig. 2 shows a comparison of top view and cross-sectional SEM images of three different ZrCu TFMGs namely: $Zr_{24}Cu_{76}$ (Fig. 2a-1, a-2); $Zr_{52}Cu_{48}$ (Fig. 2b-1, b-2); $Zr_{61}Cu_{39}$ (Fig. 2c-1, c-2). Fracture surfaces generated from cleavage of the silicon wafer substrate (Fig. 2a-2, b-2, c-2) show a vein-like morphology characteristic of metallic glasses as a further indication of the amorphous nature of the films [3]. The $Zr_{24}Cu_{76}$ film displays homogeneous morphology (Fig. 2a-1, a-2), however, films with Cu content below 50 at.%, such as $Zr_{52}Cu_{48}$ (Fig. 2b-1, b-2) and $Zr_{61}Cu_{39}$ (Fig. 2c-1, c-2), show presence of a nanostructured columnar morphology with an average column diameter of $\sim$ 20–50 nm, which are also visible in the top-view SEM images (Fig. 2b-1, c-1). Even though this morphology resembles that of a nanocrystalline film, the XRD spectra (Fig. 1) do not show any presence of crystallization.

The presence of the columnar nanostructure for these Zr-rich compositions can be related to the relatively lower power applied to the RF cathode on which the Cu target was mounted, compared to Cu-rich films. This, combined with the relatively large target to substrate distance (i.e. 239 mm) would cause a less homogeneous flux of the sputtered atoms, that reach the substrate with lower energy leading to cluster growth and consequently to a columnar structure, as also reported by other studies, on Au-based or Ni-Nb TFMGs [17,18]. Despite the presence of a columnar nanostructure visible in SEM secondary electron images, all films possess a mirror-like surface, indicating a very low surface roughness. This was confirmed through AFM measurements, showing that the root mean square (rms) roughness has comparable values for both homogeneous $Zr_{24}Cu_{76}$ (i.e. 1.1 nm) and nanocolumnar $Zr_{52}Cu_{48}$ (i.e. 0.9 nm) and $Zr_{61}Cu_{39}$ films (i.e. 0.9 nm) (Fig. 2).

The nanocolumnar morphology of $Zr_{52}Cu_{48}$ and $Zr_{61}Cu_{39}$ resembles that of nanoglasses (NGs), a class of metallic glasses structurally modified showing different amorphous "grains" separated by amorphous interfaces. Experimental works and MD simulations on ZrCu NGs, have shown that the glass-glass interfaces possess a different atomic order as well as a higher free volume compared to the core glass regions [16,19–21].

To study the effect of composition and nanostructure on the mechanical properties of ZrCu TFMGs, three compositions were studied in more detail: *i.e.* $Zr_{24}Cu_{76}$, $Zr_{52}Cu_{48}$ and $Zr_{61}Cu_{39}$. This is rationalized as these three compositions belong to different regions of the amorphous-ZrCu system, the middle of the amorphization range ($Zr_{52}Cu_{48}$), the boundaries of Zr-rich ($Zr_{61}Cu_{39}$) and Cu-rich ($Zr_{24}Cu_{76}$) amorphous regions. Therefore, more pronounced compositional effects on the thermal and mechanical properties of ZrCu are to be expected.

3.2. Thermal stability and crystallization phenomena

Fig. 3a shows the evolution of the atomic structure, investigated by XRD, as a function of temperature between T_{room} and 600 °C for a film with composition $Zr_{52}Cu_{48}$. Similar graphs for $Zr_{24}Cu_{76}$ and $Zr_{61}Cu_{39}$ can be found in the Supplementary Information (Fig. S2). For all three studied compositions (*i.e.* $Zr_{24}Cu_{76}$, $Zr_{52}Cu_{48}$ and $Zr_{61}Cu_{39}$), the amorphous structure remains stable to at least 300 °C. From this temperature, crystallization starts to occur, initially preceded by surface oxidation phenomena evidenced through the emergence at low 2θ angles (i.e. $\sim$ 27° in Fig. 3a) of a ZrO_2 peak, despite the use of a controlled He atmosphere. However, as seen from Fig. 3b, the sensitivity toward oxidation depends on film composition, with a higher resistance for $Zr_{52}Cu_{48}$, where oxidation appears only at 360 °C. In Fig. 3b the crystallization tem-
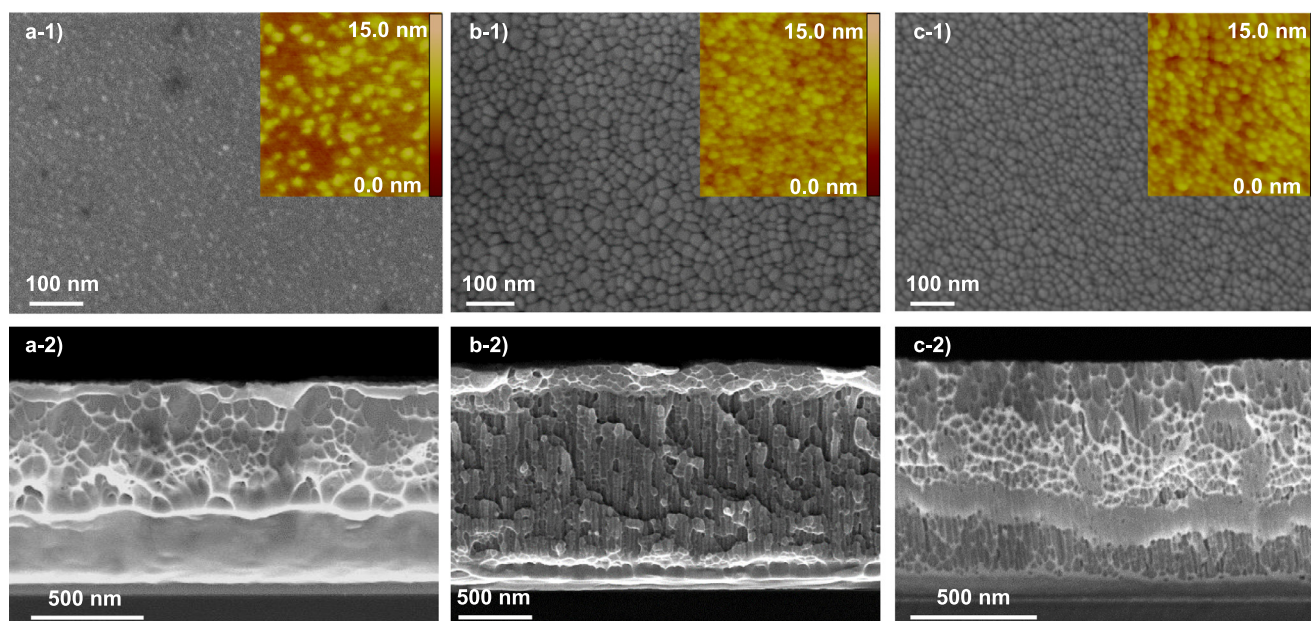

Fig. 2. Morphology of ZrCu TFMGs: (top) SEM top view (bottom) and cross-section images of film fracture surface morphologies of $Zr_{24}Cu_{76}$ (a-1, a-2), $Zr_{52}Cu_{48}$ (b-1, b-2) and $Zr_{61}Cu_{39}$ (c-1, c-2) films. Insets in top view images show AFM scans of the corresponding surfaces; scale bars for SEM plane view and AFM images are the same. The typical metallic glass vein-like fracture surface pattern is found for all compositions, while a columnar nanostructured morphology is shown for $Zr_{52}Cu_{48}$ (b-1, b-2) and $Zr_{61}Cu_{39}$ (c-1, c-2).
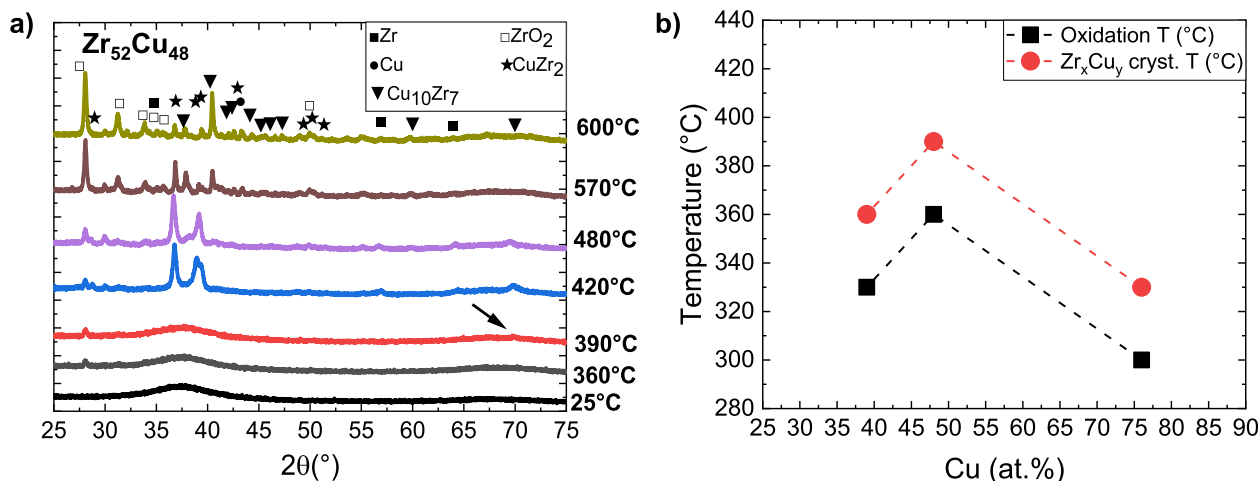
Fig. 3. Thermal resistance against crystallization: (a) XRD spectra of $Zr_{52}Cu_{48}$ as a function of temperature. Oxidation occurs with formation of ZrO_2 crystals at 360 °C, while intermetallic phases start to appear from 390 °C, as indicated by the black arrow; (b) evolution of the oxidation and crystalitzation temperatures as a function of film composition.

perature (T_x) of ZrCu TFMGs is observed to initially increase with Cu content, in good agreement with literature [11,29,30]. However, structural stability of the glass phase for ZrCu alloys is expected to show a maximum between 48 and 70 at.% Cu [11], as also confirmed by the presented results on $Zr_{52}Cu_{48}$ showing the highest T_x among the three compositions studied. The highest thermal stability within the 48–70 at.% Cu range has several justifications. From a thermodynamic point of view, formation enthalpy (ΔH) of amorphous ZrCu has a minimum around 50 at.% Cu, which translates in higher stability of the glass phase and therefore higher resistance toward crystallization [31].

Moreover, thermal stability of the ZrCu amorphous phase can be also related to the particular atomic packing within the 48–70 at.% Cu composition interval. Indeed, while amorphous, metallic glasses exhibit a local atomic order within which neighboring atoms can form clusters and various coordination polyhedra [32]. The topology and the volume fraction occupied by the formed polyhedra are reported to be dependent on ZrCu composition. In particular, glass forming ability has been linked to presence of pentagonal Zr–centered clusters, which has a maximum around 65 at. % Cu, making these compositions less prone to devitrification [12,13].

Interestingly, the presence of nanocolumns and glassy interfaces seem not to affect the thermal stability of $Zr_{52}Cu_{48}$ and Zr_{61}-Cu_{39}. Indeed, the nanostructured films show T_x values similar to reports by Apretusei *et al.* using equivalent high temperature XRD measurements [11], indicating that thermal stability of the films is mainly affected by the strength of Zr-Cu bonds and the composition.

When Cu content increases, for $Zr_{24}Cu_{76}$ films T_x drops to much lower values (i.e. 330 °C, Fig. 3b). This can be attributed to a further change in the atomic packing distribution and free volume caused by the higher amount of Cu. Indeed, the volume fraction of icosahedral clusters continues to increase with Cu content (but only to $\sim$ 75 at.% Cu), while the concentration of Zr–centered clusters beneficial to glass forming ability start to already decrease from $\sim$ 60 at.% Cu, affecting the structural stability of Cu-rich alloys.

Strengthening this assertion, $Zr_{24}Cu_{76}$ is the only composition for which a sharp and intense Cu peak corresponding to the fcc (200) phase appears from 330 °C (see Fig. S2). Furthermore, Zr_{24}-Cu_{76} has both the lowest oxidation and crystallization temperatures among the alloys examined in this study, occurring respectively at 300 °C and 330 °C (Fig. 3b).

3.3. Elastic properties and nanoindentation hardness

The hardness (H) of ZrCu TFMGs was evaluated using continuous stiffness measurement (CSM) nanoindentation, while for elastic properties, a comparison between nanoindentation and surface Brillouin spectroscopy (SBS) was made. Nanoindentation values of H and elastic modulus (E) were evaluated for 1 μm thick $Zr_{24}Cu_{76}$, $Zr_{52}Cu_{48}$ and $Zr_{61}Cu_{39}$ films, at penetration depths between $\sim$ 5–10% and $\sim$ 4.5–7% of their film thickness, respectively.

Fig. 4a shows the effect of composition on H and E evolution. It can be noticed that E initially drops from $\sim$ 87 GPa to $\sim$ 76 GPa for films with 5 at.% and 26 at.% Cu, as a consequence of the transition from crystalline to amorphous structure. In contrast, within the amorphous interval (marked by the grey background in Fig. 4a) both E and H increase with Cu content, respectively, from 4.6 up to 7.7 GPa and from 76 up to 116 GPa, in good agreement with other studies on sputtered ZrCu TFMGs [7,33,34]. This behavior can be explained by the shortening of interatomic distances and the denser atomic packing, as Cu content increases, which induces the increase in E [7]. This is in agreement with the shift of the diffraction hump toward higher 2θ (Fig. 1). Additionally, it has been shown that the formation of full-icosahedral atomic packing increasing the Cu at. %, which induces higher resistance toward shear instability, and further supporting the increment of H [8,9].

Presence of nanocolumnar structure, for $Zr_{52}Cu_{48}$ and $Zr_{61}Cu_{39}$, seems not to play a key role for the values of E and H, which are comparable to those reporteded in literature for films with similar compositions, but compact morphologies [7,33,34]. Further, it is observed that despite the presence of very fine interfaces, within the film nanostructure (possibly associated with higher free volume content), the average atomic distances, obtained from XRD (see Fig. 2 and Fig. S1) are equivalent to those of homogeneous films from other studies [7,34]. Therefore, it can be concluded that in a first approximation, the mechanical behavior is mainly dictated by the intimate atomic structure and strength of Zr-Cu bonds even if a fine nanocolumnar structure is present.

To have a more complete investigation of elastic properties, nanoindentation results were compared with SBS. The latter technique, based on laser interaction with surface acoustic waves, is able to provide an accurate measure of elastic constants with the advantage of not being affected by the presence of a substrate [35]. Illustration of representative Brillouin spectra measured on $Zr_{52}Cu_{48}$ and their fitting are shown in the Fig. S5. The Rayleigh surface wave frequency (R) increases continuously versus the Cu
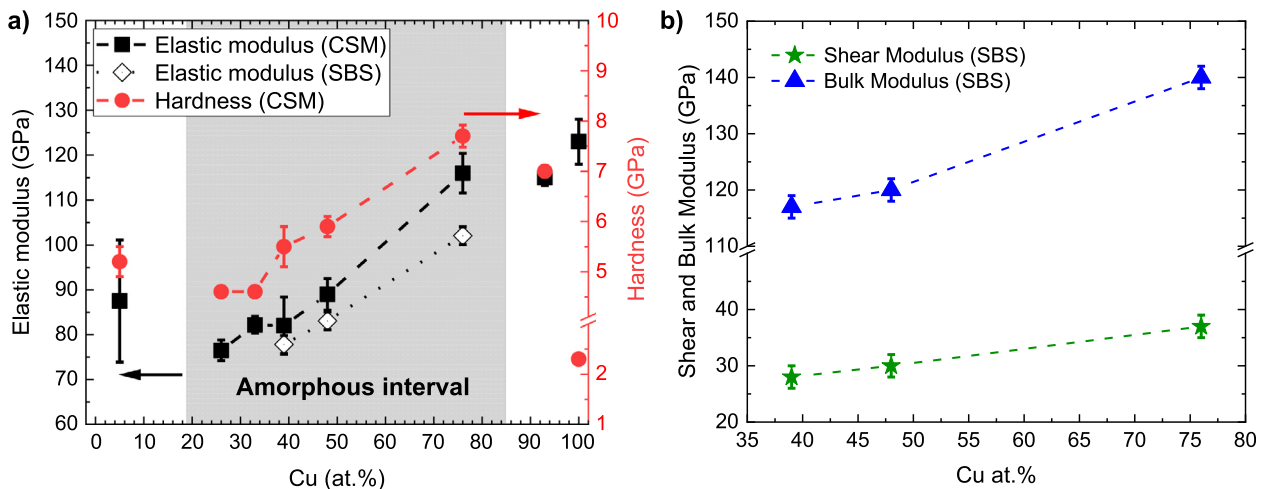
Fig. 4. Effect of composition on elastic moduli and hardness: (a, b) evolution of the elastic and shear moduli (extracted by nanoindentation and surface Brillouin spectroscopy) and H, as a function of Cu content. All quantities increase within the amorphization interval for Cu-rich specimens.

content; consequently, Rayleigh surface wave sound velocity (V_R- ~ βV_S) and shear wave velocity (V_S) increase as well. The variation of the shear velocity is affected by the relative change in mass density and, thus, does not reflect in a direct way the evolution of the shear elastic constant. As mass density monotonously increases with Cu concentration (*i.e.* from 7.45 g/cm^3 to 8.36 g/cm^3 for Zr$_{61}$-Cu$_{39}$ and Zr$_{24}$Cu$_{76}$ compositions), it is deduced that the shear modulus $C_{44} = \rho V_S^2$ also increases as reported in Fig. 4b. The remaining C_{11} elastic constant (through which E and Poisson's ratio can be calculated) is determined from the fitting of Sezawa surface wave (S_i) frequency positions. As expected from the decrease in the average interatomic distance (Fig. 1 and Fig. S1), E increases with Cu concentration (see Fig. 4a) while Poisson's ratio remains roughly constant and equal to ~ 0.38 (Table S3).

This increase of shear constant C_{44} with addition of Cu is clearly correlated to a strengthening of the plastic deformation resistance [36]. Besides, Plummer *et al.* [37] demonstrated that the ratios of elastic constants C_{44}/C_{11} and C_{12}/C_{11} can qualitatively describe basic glassy properties for bulk metallic glasses, such as the fragility or interatomic bonding. For ZrCu TFMGs C_{44}/C_{11} and C_{12}/C_{11} remain close to values of 0.2 and 0.6, respectively (See Table S1). This corresponds to a fragile-intermediate metallic glass behavior, above the covalent region threshold defined by the Cauchy relation $C_{12} = C_{44}$, valid for central force acting between atoms (see Fig. S6), similar to amorphous MoSi films [27]. The shear over bulk modulus ratio (or Pugh's ratio, G/B) remains between ~ 0.24–0.27, i.e. below the brittle threshold value for amorphous materials, and therefore plastic deformation is expected [26,38]. The Cauchy pressure is positive, indicating a metallic bond character and potential for plastic deformability [39].

The energetic driving force and resistance for shearing and cracking in metallic glasses has been quantitatively evaluated by Liu *et al.* [40] with a thermodynamic criterion, the cooperation parameter $\delta = (1 + \nu)^2/12.65(1-2\nu)^2$, for better understanding the intrinsic correlations between fracture toughness and Poisson's ratio. This quantitatively depicts the relative propensity of shearing ($\delta > 1$) versus cracking ($\delta < 1$). The ZrCu films here investigated have $\delta \sim 1.5–1.9$ (see Table S1), again indicating an aptitude for plastic deformability.

3.4. Load dependent deformation and serrated flow behavior during nanoindentation

To study the deformation and serrated flow behavior of ZrCu TFMGs, standard nanoindentation measurements were performed using different loading rates (i.e. from 25 mN/s down to 1.67 mN/s). The load–displacement (*P-h*) curves for 1 µm thick Zr$_{24}$Cu$_{76}$, Zr$_{52}$Cu$_{48}$ and Zr$_{61}$Cu$_{39}$ films are shown in Fig. 5.

When high load rates are applied (Fig. 5a), no evident sign of serrated flow is present except for Zr$_{61}$Cu$_{39}$. However, once the load rate is decreased (Fig. 5b,c,d) serrations start to appear in the form of sudden bursts of displacement increase at constant load. In metallic glasses serrated flow is proven to be directly linked to plastic deformation through the formation of shear bands [3]. It has also been reported how indentation load rate below a critical threshold would allow metallic glasses to accommodate deformations through local atomic rearrangement occurring with the activation of single shear bands [41]. Consequently, this gives rise to serrated flow to appear in the form of displacement bursts in the *P-h* curves (Fig. 5b). However, at indentation speeds above the critical value, one single localized shear band will not be able to quickly accommodate the applied strain, therefore multiple shear bands must be generated and serrated flow is suppressed. Therefore, the *P-h* curves appear more uniform (Fig. 6a). Noticeably, the critical load rate for appearance of serrations depends on the ZrCu composition and nanostructure (Fig. 5). Zr$_{61}$Cu$_{39}$ shows clear signs of serration at 10 mN/s (Fig. 5b), while for Zr$_{52}$Cu$_{48}$ and Zr$_{24}$Cu$_{76}$ (i.e. the latter shows a homogeneous morphology) they start to appear only at lower load rates (i.e. 5 and 1.67 mN/s, Fig. 5c, d).

Further, the nanoindentation strain rate curves can be examined (Fig. 6), following the methodology in Ref. [41]. When a constant load rate is applied, strain rate varies during indentation following a non-linear monotonic decreasing function of time, or equivalently, of indentation depth. This can be described by $\varepsilon_i = (1/h)(dh/dt)$, where h corresponds to penetration depth and t to time [42].

However, strain rate curves in Fig. 6 show several peaks and no continuous monotonic tendency. These peaks represent rapid accelerations of the strain rate, which are directly linked to the bursts present in load–displacement (*P-h*) curves and serrated flow events in Fig. 5 [41]. From Fig. 6 it is observed that peak heights increase for lower loading rates, but also that film composition has an influence on strain rate: Zr$_{61}$Cu$_{39}$ shows higher peaks for each of the considered indentation velocities (Fig. 6a). This can be quantified by evaluating the strain rate peak intensity $A = \varepsilon_{i,max}/\varepsilon_{i,base}$, as the ratio between maximum peak height (*i.e.* $\varepsilon_{i, max}$) and baseline strain rate value at the peak location (*i.e.* $\varepsilon_{i, base}$). Therefore, peak intensity (*A*) represents the factor by which the deformation is accelerated during serrated flow [41].
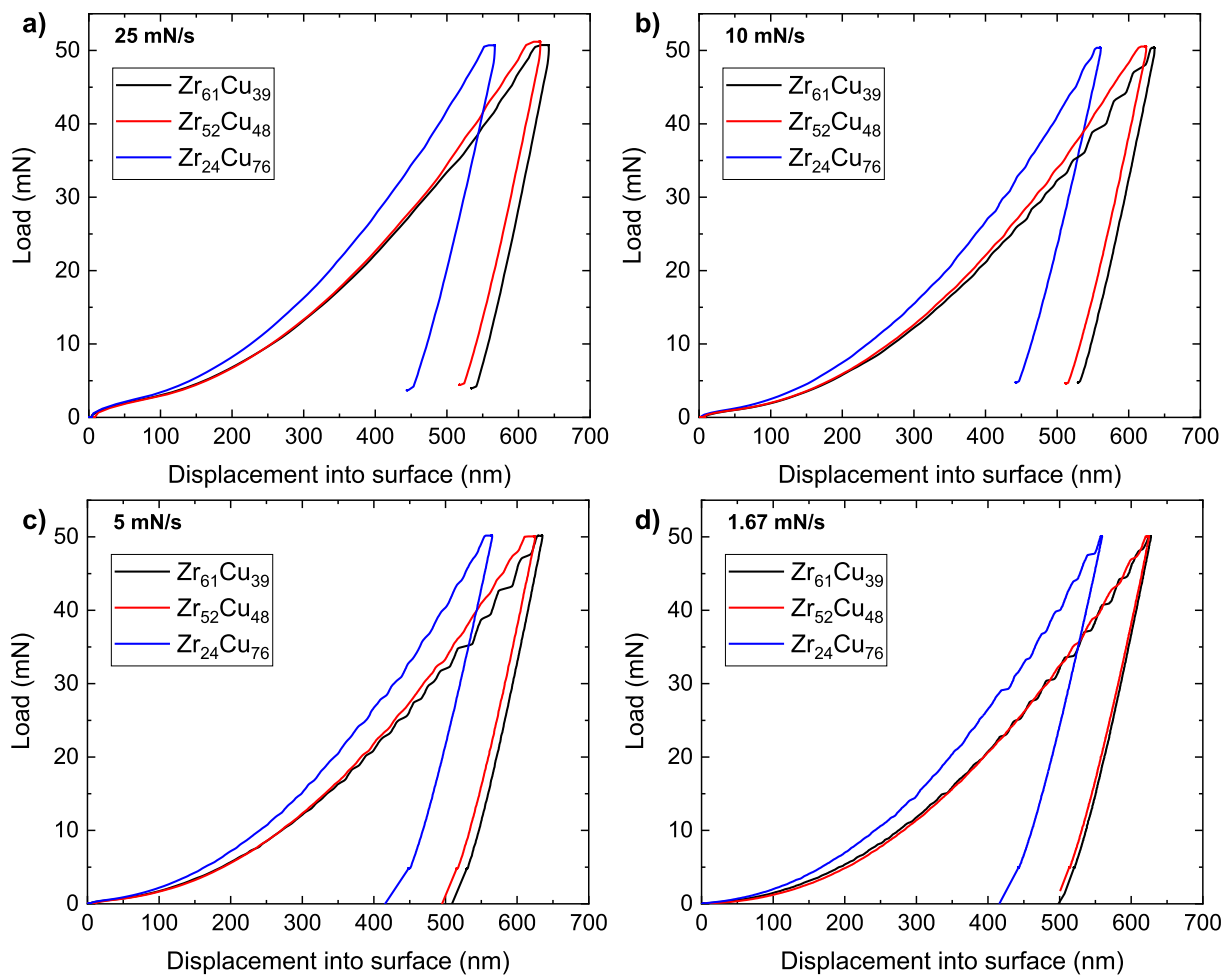
Fig. 5. Serrated flow behavior dependence on composition: nanoindentation load–displacement (P-h) curves with decreasing load rate values from (a) to (d). As load rate decreases, single serrated flow events become more evident through the appearance of displacement bursts at constant loads. The Zr-rich $Zr_{61}Cu_{39}$ is the most prone to serrated flow, which is already evident at higher load reate values (i.e. 10 mN/s, Fig. 5b) than for $Zr_{24}Cu_{76}$ and $Zr_{52}Cu_{48}$.
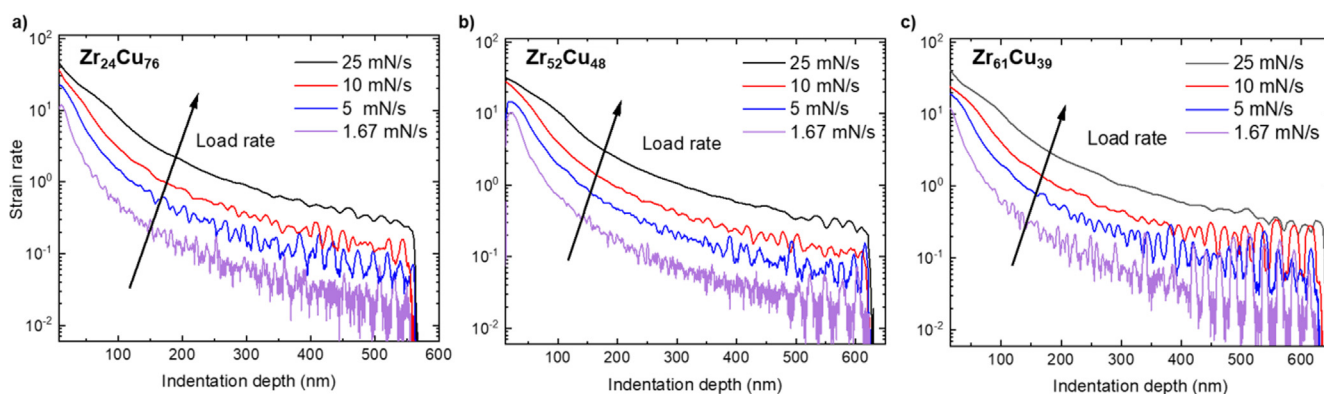

Fig. 6. Strain rate curves as function of composition and load rate: peaks in strain rate curves represents sudden accelerations in deformation speed coinciding with serration (strain bursts) events. Peak intensities generally increase when load rate decreases and at higher penetration depths. It is noted that $Zr_{61}Cu_{39}$ (c) peaks are much larger compared to those for $Zr_{24}Cu_{76}$ and $Zr_{52}Cu_{48}$ (a, b) for the same load rate values.

From curves in Fig. 7a, which show the average strain rate peak intensity (*A*) as function of loading rate, it is further noted how *A* increases for all three ZrCu compositions with decreasing loading rate. Nevertheless, except for the case of 25 Nm/s, $Zr_{61}Cu_{39}$ always exhibits larger *A* values than both other compositions; a further indication that it is more prone to form serrations and undergo to shear band deformation. Finally, comparing average serration sizes (Fig. 7) it is observed that they remain constant within error as a function of loading rate, while composition have an evident effect; films with lower Cu content present larger serration sizes. Since serrations can be directly related to micro-plastic deformation events [43], this last result suggests that film composition can control not only plastic deformation and serrated flow behavior, but also the size of microplastic deformations.
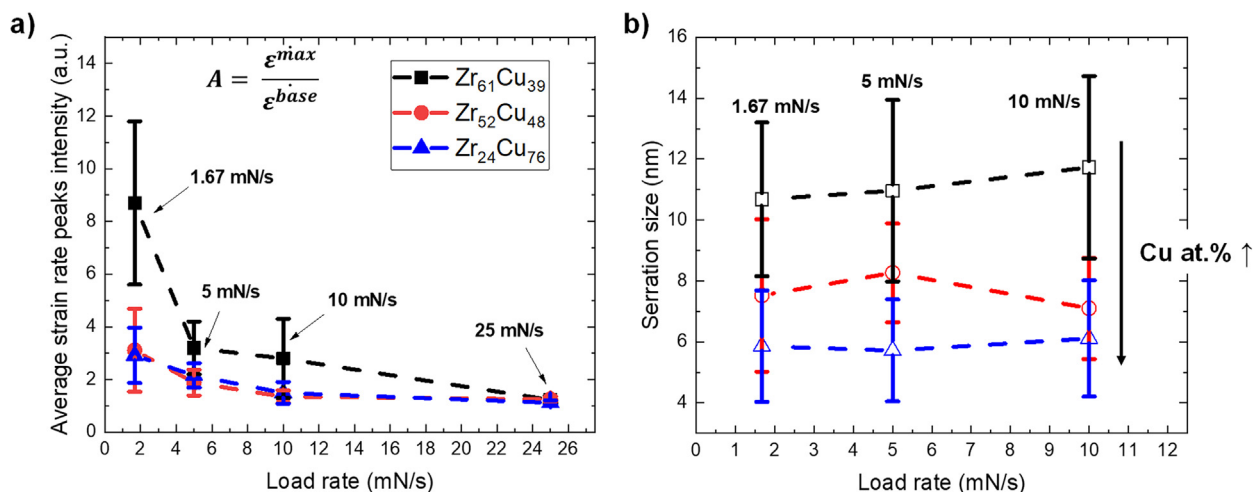
Fig. 7. Analysis of serrated flow as a function of ZrCu film composition: (a) plot of average values of strain rate peak intensities calculated for all the different nanoindentation loading rates (referring to strain rate curves in Fig. 5). Peak intensities are highest for films with $Zr_{61}Cu_{39}$ composition; (b) comparison of average serration sizes. Serrated flow events are larger for compositions with lower elastic modulus/hardness.

However, to have a better understanding of these results it is necessary to discuss both the role of TFMGs composition and also of the different morphologies, namely homogeneous and nanocolumnar. First, effect of composition is considered, resulting in different atomic packing.

Specifically, Cu-enrichment induces a different local atomic ordering together with variation in average atomic distance, therefore affecting the deformation capacity of the films. MD simulations on ZrCu metallic glasses have shown that Cu content can control the local atomic order, inducing an increase of full icosahedral packing for Cu-rich glasses, which is linked to higher resistance to shear instabilities [8,9]. This strongly aligns with the results, which show that films richer in Cu have higher resistance against serrated flow.

On the other hand, it can be considered that a higher content of free volume is expected due to the presence of glass-glass interfaces [16,19-21] within the nanocolumnar structure. Free volume in MGs structure, has been indicated as the primary source for shear transformation zones (STZs), from which SBs can nucleate [3,44]. Therefore, the higher free volume content could justify the larger plasticity due to micro-SBs activation for nanocolumnar TFMGs, which translates to a higher tendency toward serrated flow observed for nanostructured morphologies [44]. Nandam *et al.* [16] reported on $Zr_{50}Cu_{50}$ nanoglasses (NGs), showing nanoindentation curves without presence of serrated flow in contrast to melt-spun MGs with homogeneous morphology. This was rationalized by the large free volume content at the interfaces between the different amorphous grains, enabling the simultaneous nucleation of micro-SBs inducing a homogenous deformation of the NGs. However, it is worth to highlight the difference between the columnar nanostructure obtained here by magnetron sputtering deposition and the one of NGs obtained by inert gas condensation (IGC) followed by high pressure compaction of the amorphous powder. Indeed, in NGs free volume is homogeneously distributed among their structure and can be associated to density fluctuations between the dense amorphous cores and the interface regions with lower atomic density and higher free volume content [16]. Therefore, upon loading, nucleation of multiple micro-SBs could be homogeneously distributed within the NGs structure, leading to uniform deformation and smooth nanoindentation curves.

This is however different for nanocolumnar TFMGs, where the free volume rich interfaces would be located at the boundaries between the vertically aligned nanocolumns. Consequently, in this case free volume would not be distributed within the material as in NGs, but rather more confined, favoring the nucleation of single SBs. Therefore, this could justify the localized plastic deformation and serrated flow behavior during nanoindentation (as in Fig. 5). In addition, MD simulations have shown how mechanical properties of ZrCu NGs depends on the size of their nanostructure [20,21]. Indeed, only NGs with grain sizes below 5 nm show homogeneous deformation, while NGs with larger grains showed nucleation of localized SBs [20,21].

3.5. Crack and buckle evolution: Tensile tests on flexible substrates

Fig. 8 shows the surface evolution of damage for 400 nm thick ZrCu films deposited on Kapton® substrates for three deformation states: initial state, beginning of multi-fissuring, and buckling. The experiments initially show an increase of crack density with applied strain, followed by the initiation and multiplication of buckles perpendicular to the straining direction due to differences in lateral contraction of Kapton and ZrCu films [45]. The quantification of crack and buckle densities as a function of external strain are shown in Fig. 9. Fig. 9a shows the crack density as a function of strain for the three compositions. Appearance of the first cracks occurs at low deformation strains for $Zr_{52}Cu_{48}$ and $Zr_{61}Cu_{39}$ (~0.5%), while it is delayed for Cu-rich $Zr_{24}Cu_{76}$ film (~2.1%). A first explanation of this delay with increasing Cu content could be a difference in the residual stress state. However, by performing an order of magnitude calculation using the elastic constants measured by SBS, this would correspond to a difference of ~1.5 GPa between $Zr_{24}Cu_{76}$ and the other two compositions, which is not reasonable based on the small difference in power supply used on Cu-Zr targets.

As discussed in Section 3.1, the AFM measurements show that rms roughness values are comparable and very low (~1 nm) for both nanocolumnar and homogeneous films. In addition, the analysis on crack spacing distribution show that crack bounding ratio is equal to 2.1 and also that ratio between adjacent cracks spacing always fall between values of 1 and 2 for all the films. This fulfills the criteria for shear lag suggested by Taylor et al. [46]; accordingly, it is possible to exclude effects of surface roughness or film unevenness on the tensile test results.

Therefore, the explanation for the different cracking onsets is likely found in an increased stiffness (*i.e.* elastic modulus) and corresponding work of separation for $Zr_{24}Cu_{76}$ due to the Cu enrich-
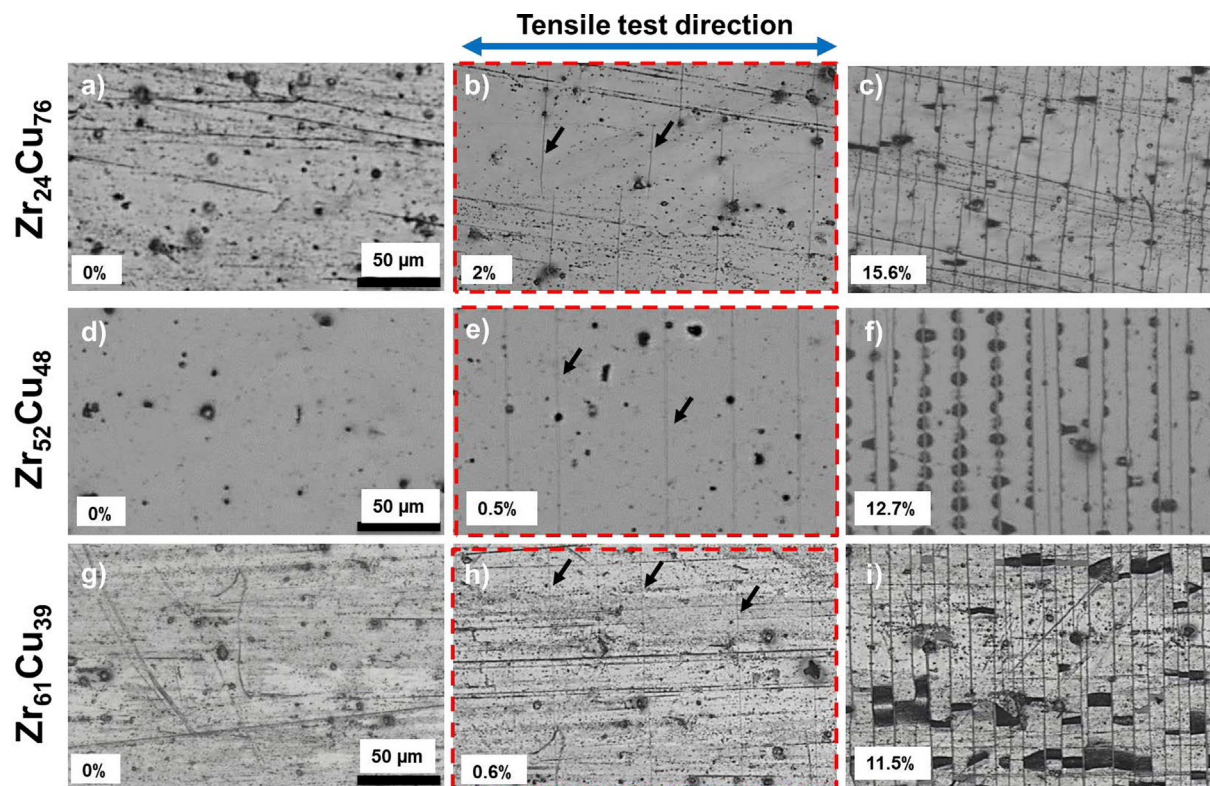
Fig. 8. Top view optical images of crack evolution during tensile testing of ZrCu films deposited on Kapton® substrates: from top to bottom (a, b, c) $Zr_{24}Cu_{76}$, (d, e, f) $Zr_{52}Cu_{48}$ and (g, h, i) $Zr_{61}Cu_{39}$. The vertical left side of the panel shows images of the films before strain is applied. Images in the central part, highlighted with red frames, show elongations at which the coatings begin to crack. Cracks form perpendicular to the direction of tensile strain. On the right side are images of the samples after the appearence of buckling events. (For interpretation of the references to colour in this figure legend, the reader is referred to the web version of this article.)
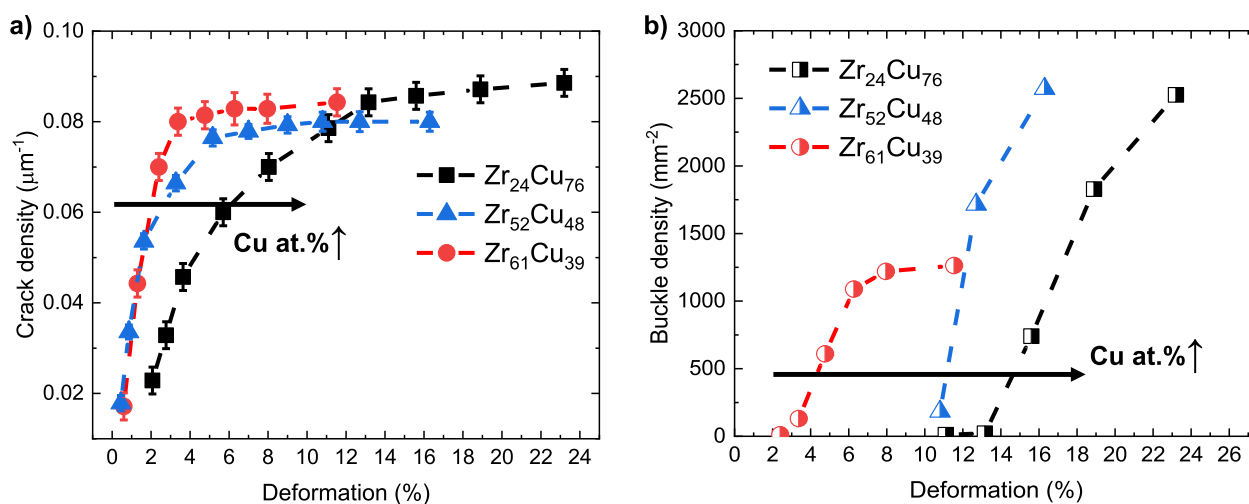

Fig. 9. Resistance to cracking and buckling of ZrCu films deposited on flexible polymer substrates: (a) crack and (b) buckle density curves as a function of the applied deformation. Both data show that with increasing Cu content resistance against crack formation and buckling increases.

ment. This is in good agreement with results presented in the previous section and the respective discussion. The larger volume fraction of full icosahedral atomic packing present in Cu-rich ZrCu TFMGs increases their mechanical strength, due to the better resistance of this structural configuration against shear instabilities [8,9], and allows the films to better resist crack propagation. In addition to this, the interfaces between the nanocolumns of Zr_{52}-Cu_{48} and $Zr_{61}Cu_{39}$ films could present preferential crack initiation sites [47], and therefore further lower the resistance of the films richer in Zr.

Similarly, Fig. 9b shows the evolution of buckle surface density with applied tensile strain due to lateral constriction. It was found that the Cu-rich and homogeneous sample (i.e. $Zr_{24}Cu_{76}$) show a higher buckling strain (about 12%), in good accordance with Wu et al. [47]. This is explained by the higher film stiffness (i.e. elastic modulus), delay in tensile cracking and stronger interface adhesion [45]. In contrast, $Zr_{61}Cu_{39}$ shows a very low buckle strain, indicating low adhesion of the Zr-rich film on the Kapton substrate.

These results show that the control of composition and nanostructure can help the design of TFMGs with higher cracking

resistance and more compatible properties for applications such as flexible electronics.

4. Conclusion

In this work the effects of composition and nanostructure on mechanical properties and thermal stability of ZrCu TFMGs have been investigated and compared to the existing literature. It is showed that the presence of columnar nanostructure does not have a large influence on elastic modulus, hardness and crystallization temperature, which instead are mainly governed by film composition which controls both average atomic distances and local atomic order.

On the other hand, investigations on the plastic, viscoplastic and fracture resistance show how these parameters are influenced by both composition and nanostructure. Specifically, it is proposed that nanostructured Zr-rich films with expected larger free volume content and interfaces, together with a lower fraction of full icosahedral atomic packing, are more prone to the nucleation of single SBs with deformation through serrated flow during nanoindentation and lower cracking resistance during tensile tests on flexible substrates. In particular it was shown that:

- Despite their columnar nanostructure, and the expected larger free volume content of glass-glass interfaces, $Zr_{52}Cu_{48}$ and $Zr_{61}Cu_{39}$ show higher thermal resistance against crystallization than Cu-rich $Zr_{24}Cu_{76}$ film, in good agreement with literature. This indicates that local atomic order, in particular the larger presence of Zr-centered atomic clusters, has larger impact on the thermal stability for the amorphous phase.
- Films with a nanostructured morphology do not show significant differences in elastic modulus and hardness values (i.e. compared to homogeneous films with similar compositions), which continuously increase with Cu at.% content (i.e. between 26 and 76 at.%) due to the induced decrease of atomic distances and the increase in presence of full-icosahedral atomic packing.
- On the other hand, viscoplasic behavior and plastic deformability are influenced by both film composition and nanostructure. Homogeneous Cu-rich films have a higher resistance toward serrated flow, due to the larger presence of stable full-icosahedral atomic packing, while nanostructured Zr-rich films show higher tendency to form SBs and to serrated flow, due to the expected larger presence of free volume located at columns interfaces and the lower fraction of full-icosahedral atomic packing.
- Similarly, Cu-rich films deposited on flexible substrates show higher fracture resistance during tensile deformation, remaining uncracked up to 2.1% strain; while interfaces of nanostructured films favor crack nucleation.

These findings confirm the key role of composition in controlling the structure and mechanical properties of ZrCu TFMGs, and highlight how the nanostructure can also play a role in the plastic deformation behavior. This not only underlines that structure and properties of amorphous metallic films are intrinsically related, but also how it is possible to rationally tune the mechanical behavior of TFMGs, improving their suitability for myriad of applications.

Declaration of Competing Interest

The authors declare that they have no known competing financial interests or personal relationships that could have appeared to influence the work reported in this paper.

Data Availability

The raw/processed data required to reproduce these findings cannot be shared at this time as the data also forms part of an ongoing study.

Appendix A. Supplementary material

Supplementary data to this article can be found online at https://doi.org/10.1016/j.matdes.2022.110752.

References

[1] M. Telford, The case forbulk metallic glass, Mater. Today 7 (3) (2004) 36–43.
[2] A.L. Greer, Y.Q. Cheng, E. Ma, Shear bands in metallic glasses, Materials Science and Engineering: R: Reports 74 (4) (2013) 71–132.
[3] C. Schuh, T. Hufnagel, U. Ramamurty, Mechanical behavior of amorphous alloys, Acta Mater. 55 (12) (2007) 4067–4109.
[4] C.A. Volkert, A. Donohue, F. Spaepen, Effect of sample size on deformation in amorphous metals, J. Appl. Phys. 103 (8) (2008) 083539, https://doi.org/10.1063/1.2884584.
[5] M. Ghidelli, H. Idrissi, S. Gravier, J.-J. Blandin, J.-P. Raskin, D. Schryvers, T. Pardoen, Homogeneous flow and size dependent mechanical behavior in highly ductile Zr65Ni35 metallic glass films, Acta Mater. 131 (2017) 246–259.
[6] S. Lee, S.-W. Kim, M. Ghidelli, H.S. An, J. Jang, A.L. Bassi, S.-Y. Lee, J.-U. Park, Integration of Transparent Supercapacitors and Electrodes Using Nanostructured Metallic Glass Films for Wirelessly Rechargeable, Skin Heat Patches, Nano Lett 20 (7) (2020) 4872–4881.
[7] M. Apreutesei, P. Steyer, L. Joly-Pottuz, A. Billard, J. Qiao, S. Cardinal, F. Sanchette, J.M. Pelletier, C. Esnouf, Microstructural, thermal and mechanical behavior of co-sputtered binary Zr–Cu thin film metallic glasses, Thin Solid Films 561 (2014) 53–59.
[8] Y.Q. Cheng, A.J. Cao, H.W. Sheng, E. Ma, Local order influences initiation of plastic flow in metallic glass: Effects of alloy composition and sample cooling history, Acta Mater. 56 (18) (2008) 5263–5275.
[9] Y.Q. Cheng, H.W. Sheng, E. Ma, Relationship between structure, dynamics, and mechanical properties in metallic glass-forming alloys, Physical Review B 78 (1) (2008), https://doi.org/10.1103/PhysRevB.78.014207.
[10] P. Zeman, M. Zítek, Š. Zuzjaková, R. Čerstvý, Amorphous Zr-Cu thin-film alloys with metallic glass behavior, J. Alloy. Compd. 696 (2017) 1298–1306.
[11] M. Apreutesei, P. Steyer, A. Billard, L. Joly-Pottuz, C. Esnouf, Zr–Cu thin film metallic glasses: An assessment of the thermal stability and phases' transformation mechanisms, J. Alloy. Compd. 619 (2015) 284–292.
[12] K.-W. Park, J.-i. Jang, M. Wakeda, Y. Shibutani, J.-C. Lee, Atomic packing density and its influence on the properties of Cu–Zr amorphous alloys, Scr. Mater. 57 (9) (2007) 805–808.
[13] H.L. Peng, M.Z. Li, W.H. Wang, C.-Z. Wang, K.M. Ho, Effect of local structures and atomic packing on glass forming ability in CuxZr100−x metallic glasses, Appl. Phys. Lett. 96 (2) (2010) 021901, https://doi.org/10.1063/1.3282800.
[14] M. Ghidelli, A. Orekhov, A.L. Bassi, G. Terraneo, P. Djemia, G. Abadias, M. Nord, A. Béché, N. Gauquelin, J. Verbeeck, J.-P. Raskin, D. Schryvers, T. Pardoen, H. Idrissi, Novel class of nanostructured metallic glass films with superior and tunable mechanical properties, Acta Mater. 213 (2021) 116955, https://doi.org/10.1016/j.actamat.2021.116955.
[15] Y. Ivanisenko, C. Kübel, S.H. Nandam, C. Wang, X. Mu, O. Adjaoud, K. Albe, H. Hahn, Structure and Properties of Nanoglasses, Adv. Eng. Mater. 20 (12) (2018) 1800404, https://doi.org/10.1002/adem.v20.1210.1002/adem.201800404.
[16] S.H. Nandam, Y. Ivanisenko, R. Schwaiger, Z. Śniadecki, X. Mu, D. Wang, R. Chellali, T. Boll, A. Kilmametov, T. Bergfeldt, H. Gleiter, H. Hahn, Cu-Zr nanoglasses: Atomic structure, thermal stability and indentation properties, Acta Mater. 136 (2017) 181–189.
[17] S.V. Ketov, R. Joksimovic, G. Xie, A. Trifonov, K. Kurihara, D.V. Louzguine-Luzgin, Formation of nanostructured metallic glass thin films upon sputtering, Heliyon 3 (1) (2017) e00228, https://doi.org/10.1016/j.heliyon.2016.e00228.

[18] N. Chen, R. Frank, N. Asao, D.V. Louzguine-Luzgin, P. Sharma, J.Q. Wang, G.Q. Xie, Y. Ishikawa, N. Hatakeyama, Y.C. Lin, M. Esashi, Y. Yamamoto, A. Inoue, Formation and properties of Au-based nanograined metallic glasses, Acta Mater. 59 (16) (2011) 6433–6440.

[19] O. Adjaoud, K. Albe, Microstructure formation of metallic nanoglasses: Insights from molecular dynamics simulations, Acta Mater. 145 (2018) 322–330.

[20] S. Adibi, P.S. Branicio, Y.-W. Zhang, S.P. Joshi, Composition and grain size effects on the structural and mechanical properties of CuZr nanoglasses, J. Appl. Phys. 116 (4) (2014) 043522, https://doi.org/10.1063/1.4891450.

[21] S. Adibi, Z.-D. Sha, P.S. Branicio, S.P. Joshi, Z.-S. Liu, Y.-W. Zhang, A transition from localized shear banding to homogeneous superplastic flow in nanoglass, Appl. Phys. Lett. 103 (21) (2013) 211905, https://doi.org/10.1063/1.4833018.

[22] W.C. Oliver, G.M. Pharr, Measurement of hardness and elastic modulus by instrumented indentation: Advances in understanding and refinements to methodology, J. Mater. Res. 19 (1) (2011) 3–20.

[23] G. Abadias, P.h. Djemia, L. Belliard, Alloying effects on the structure and elastic properties of hard coatings based on ternary transition metal (M = Ti, Zr or Ta) nitrides, Surf. Coat. Technol. 257 (2014) 129–137.

[24] M. Ghidelli, S. Gravier, J.-J. Blandin, P. Djemia, F. Mompiou, G. Abadias, J.-P. Raskin, T. Pardoen, Extrinsic mechanical size effects in thin ZrNi metallic glass films, Acta Mater. 90 (2015) 232–241.

[25] P. Djemia, F. Ganot, P. Moch, V. Branger, P. Goudeau, Brillouin scattering investigation of elastic properties of Cu–Mo solid solution thin films, J. Appl. Phys. 90 (2) (2001) 756–762.

[26] M. Apreutesei, P. Djemia, L. Belliard, G. Abadias, C. Esnouf, A. Billard, P. Steyer, Structural-elastic relationships of Zr-TL (TL = Cu Co, Ni) thin films metallic glasses, J. Alloy. Compd. 707 (2017) 126–131.

[27] P. Djemia, A. Fillon, G. Abadias, A. Michel, C. Jaouen, Elastic properties of metastable Mo1−xSix alloy thin films: A Brillouin light scattering study, Surf. Coat. Technol. 206 (7) (2011) 1824–1829.

[28] O.P. Rachek, X-ray diffraction study of amorphous alloys Al–Ni–Ce–Sc with using Ehrenfest's formula, J. Non-Cryst. Solids 352 (36-37) (2006) 3781–3786.

[29] Z.D. Sha, Y.P. Feng, Y. Li, Statistical composition-structure-property correlation and glass-forming ability based on the full icosahedra in Cu–Zr metallic glasses, Appl. Phys. Lett. 96 (6) (2010) 061903, https://doi.org/10.1063/1.3310278.

[30] N. Mattern, A. Schöps, U. Kühn, J. Acker, O. Khvostikova, J. Eckert, Structural behavior of CuxZr100−x metallic glass (x=35−70), J. Non-Cryst. Solids 354 (10-11) (2008) 1054–1060.

[31] K. Yamaguchi, Y.-C. Song, T. Yoshida, K. Itagaki, Thermodynamic investigation of the Cu–Zr system, J. Alloy. Compd. 452 (1) (2008) 73–79.

[32] Y.Q. Cheng, E. Ma, Atomic-level structure and structure–property relationship in metallic glasses, Prog. Mater Sci. 56 (4) (2011) 379–473.

[33] Z.T. Wang, K.Y. Zeng, Y. Li, The correlation between glass formation and hardness of the amorphous phase, Scr. Mater. 65 (9) (2011) 747–750.

[34] P. Coddet, F. Sanchette, J.C. Rousset, O. Rapaud, C. Coddet, On the elastic modulus and hardness of co-sputtered Zr–Cu–(N) thin metal glass films, Surf. Coat. Technol. 206 (17) (2012) 3567–3571.

[35] D. Faurie, N. Girodon-Boulandet, A. Kaladjian, F. Challali, G. Abadias, P. Djemia, Setup for high-temperature surface Brillouin light scattering: Application to opaque thin films and coatings, Rev Sci Instrum 88 (2) (2017) 023903.

[36] S.F. Pugh, XCII. Relations between the elastic moduli and the plastic properties of polycrystalline pure metals, The London, Edinburgh, and Dublin Philosophical Magazine and Journal of Science 45(367) (2009) 823-843.

[37] J.D. Plummer, I. Todd, Implications of elastic constants, fragility, and bonding on permanent deformation in metallic glass, Appl. Phys. Lett. 98 (2) (2011) 021907, https://doi.org/10.1063/1.3540652.

[38] J.J. Lewandowski *, W.H. Wang, A.L. Greer, Intrinsic plasticity or brittleness of metallic glasses, Philos. Mag. Lett. 85 (2) (2005) 77–87.

[39] D.G. Pettifor, Theoretical predictions of structure and related properties of intermetallics, Mater. Sci. Technol. 8 (4) (1992) 345–349.

[40] Z.Q. Liu, W.H. Wang, M.Q. Jiang, Z.F. Zhang, Intrinsic factor controlling the deformation and ductile-to-brittle transition of metallic glasses, Philos. Mag. Lett. 94 (10) (2014) 658–668.

[41] C.A. Schuh, T.G. Nieh, A nanoindentation study of serrated flow in bulk metallic glasses, Acta Mater. 51 (1) (2003) 87–99.

[42] W.H. Poisl, W.C. Oliver, B.D. Fabes, The relationship between indentation and uniaxial creep in amorphous selenium, J. Mater. Res. 10 (8) (1995) 2024–2032.

[43] T.G. Nieh, C. Schuh, J. Wadsworth, Y.i. Li, Strain rate-dependent deformation in bulk metallic glasses, Intermetallics 10 (11-12) (2002) 1177–1182.

[44] N. Li, L. Liu, Q. Chen, J. Pan, K.C. Chan, The effect of free volume on the deformation behaviour of a Zr-based metallic glass under nanoindentation, J. Phys. D Appl. Phys. 40 (19) (2007) 6055–6059.

[45] M.J. Cordill, F.D. Fischer, F.G. Rammerstorfer, G. Dehm, Adhesion energies of Cr thin films on polyimide determined from buckling: Experiment and model, Acta Mater. 58 (16) (2010) 5520–5531.

[46] A.A. Taylor, V. Edlmayr, M.J. Cordill, G. Dehm, The effect of film thickness variations in periodic cracking: Analysis and experiments, Surf. Coat. Technol. 206 (7) (2011) 1830–1836.

[47] K. Wu, Y.Q. Wang, H.Z. Yuan, J.Y. Zhang, G. Liu, J. Sun, Fragmentation and adhesion properties of Cu-Zr amorphous thin films on polyimide substrates, Philos. Mag. Lett. 98 (10) (2018) 464–472.